

Dimetal Linked Open Frameworks: [(CH₃)₄N]₂(Ag₂,Cu₂)Ge₄S₁₀

Carol L. Bowes, Wendy U. Huynh, Scott J. Kirkby, Andrzej Malek,
Geoffrey A. Ozin,* Srebri Petrov, Mariusz Twardowski, and David Young

Materials Chemistry Research Group, Lash Miller Chemical Laboratories,
University of Toronto, 80 St. George Street, Toronto, Ontario, Canada M5S 3H6

Robert L. Bedard and Robert Broach

Universal Oil Products, 50 East Algonquin Road, Des Plaines, Illinois 60017-5017

Received May 15, 1996. Revised Manuscript Received May 30, 1996⁸

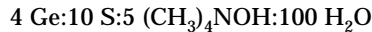
Synthetic and X-ray structural details, optical and vibrational spectroscopic, and thermal properties of the materials [(CH₃)₄N]₂M₂Ge₄S₁₀ (where M = Cu, Ag), are described for the first time. Rietveld PXRD full-profile structure refinements of [(CH₃)₄N]₂M₂Ge₄S₁₀ reveal a novel open-framework architecture in which dimetal M₂²⁺ and adamantanoid Ge₄S₁₀⁴⁻ building blocks are alternately substituted into the tetrahedral Zn²⁺ and S²⁻ sites of a zinc blende lattice, all linked together by [Ge(μ-S)]₂M-M[Ge(μ-S)]₂ metal–metal bonded bridging units. The metal–metal distances in the S₂M–MS₂ “twisted I” dihedral unit are 2.761 Å (Ag) and 2.409 Å (Cu). These internuclear separations are shorter than the bulk metals themselves (2.89 Å, Ag; 2.54 Å, Cu). This implies that the adamantanoid Ge₄S₁₀⁴⁻-based open-framework structure is held together by d¹⁰–d¹⁰ M⁺–M⁺ metal–metal bonds. FT-Raman provides a direct probe of this interaction. Dimetal-framework breathing vibrational modes are observed around 38 cm⁻¹ for M = Ag and 55 cm⁻¹ for M = Cu. *In situ* VT-PXRD analysis demonstrates that [(CH₃)₄N]₂Ag₂Ge₄S₁₀ retains its structural integrity upon exposure to air after in vacuo heating above the [(CH₃)₄N]⁺ loss temperature. It seems likely that the disilver connection of adamantanoid Ge₄S₁₀⁴⁻ building blocks confers thermal stability upon the framework.

Introduction

The compositions of self-assembling open frameworks have recently moved well beyond microporous oxides, such as aluminosilicates, silicas, and aluminophosphates, to include metals linking-up with chalcogenides, polychalcogenides, pnictides, thiopnictates, cyanides, and polydentate ligands.¹ These new frameworks have novel structure–property relationships and promise a myriad of new functions and applications.² To date their construction exclusively involves ligand binding to monomeric metal centers. We report on the synthesis and characterization of [(CH₃)₄N]₂M₂Ge₄S₁₀ (M = Ag, Cu), a class of materials in which adamantanoid Ge₄S₁₀⁴⁻ clusters are uniquely linked together by metal–metal bonded dimetal M₂²⁺ units to form an open-framework structure.

Experimental Section

The tetrameric adamantanoidal precursor³ [(CH₃)₄N]₄Ge₄S₁₀ is prepared from a reaction mixture with the relative molar composition



The product is prepared by adding, sequentially, 4.05 g of

germanium powder (99.99%, Aldrich), 4.47 g of sublimed sulfur (99.999%, Aldrich), 12.63 g of tetramethylammonium hydroxide pentahydrate (Aldrich), and 18.84 g of deionized water to a 45 mL Teflon liner. This is capped, sealed into a stainless steel bomb, and tumbled at 150 °C for 16 h. Upon cooling, trace amounts of unreacted solids are filtered off, and a deep yellow solution is recovered. Absolute alcohol and/or acetone is added to this solution until precipitation of [(CH₃)₄N]₄Ge₄S₁₀ is complete. This product is filtered, washed with ethanol then acetone, and allowed to dry under ambient conditions. Phase purity was determined by PXRD, with no evidence of any impurities, yield ca. 95%.

The [(CH₃)₄N]₂M₂Ge₄S₁₀ materials (M = Cu, Ag), were prepared by the following methods. An aqueous solution of 0.09 g of sodium thiosulfate (0.66 mmol) is made up to 1.00 g with deionized water. In a separate vial, 0.04 g of silver nitrate (0.22 mmol) is dissolved in deionized water to make up a second 1.00 g solution. The silver solution is then added to the thiosulfate solution. A tetramer solution is made up by dissolving 0.20 g of [(CH₃)₄N]₄Ge₄S₁₀ (0.22 mmol) to 2.00 g with deionized water. The tetramer solution is then added to the silver solution, mixed, and left for 16 h at 25 °C. The [(CH₃)₄N]₂Ag₂Ge₄S₁₀ product is recovered by centrifugation, (Figure 1A).

A copper solution is prepared by dissolving 0.23 g of sodium bromide (2.2 mmol) in a mixture of 1.00 g of deionized water and 1.00 g of acetonitrile followed by addition of 0.04 g (0.44 mmol) of cuprous chloride. The [(CH₃)₄N]₄Ge₄S₁₀ solution is prepared by dissolving 0.20 g of tetramer (0.22 mmol) in a mixture of 0.80 g of deionized water and 1.00 g of acetonitrile. This solution is then added to the copper solution, a fine yellow suspension forms which, after 16 h at 25 °C, yields a white precipitate. This product is recovered by centrifugation.

⁸ Abstract published in *Advance ACS Abstracts*, July 15, 1996.

(1) Bowes, C. L.; Ozin, G. A. Self-Assembling Frameworks: Beyond the Microporous Oxide. *Adv. Mater.* **1996**, *8*, 13–38 and references therein.

(2) Parise, J. B. *Science* **1991**, *251*, 293. Kanatzidis, M. G.; Park, Y. *Chem. Mater.* **1990**, *2*, 99. Ozin, G. A. *Adv. Mater.* **1992**, *4*, 612–649. Ozin, G. A. In *Materials Chemistry: An Emerging Subdiscipline*; ACS Symposium Series; Interrante, L., Ed.; Washington, DC, March 1992.

(3) Krebs, B., *Angew. Chem., Int. Ed. Engl.* **1983**, *22*, 113. Yaghi, O. M.; Sun, Z.; Richardson, D. A.; Groy, T. L. *J. Am. Chem. Soc.* **1994**, *116*, 807–808.

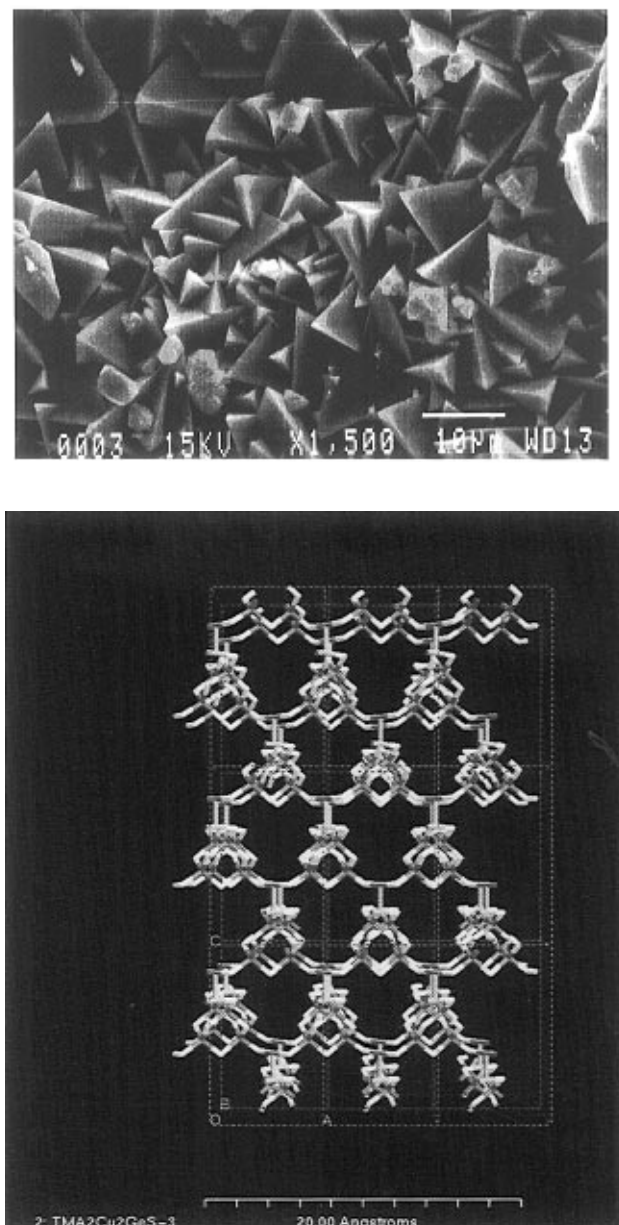


Figure 1. (A) Scanning electron micrograph image of pseudo-tetrahedral morphology crystals of $[(\text{CH}_3)_4\text{N}]_2\text{Ag}_2\text{Ge}_4\text{S}_{10}$. (B) Rietveld PXRD full-profile structure determination of $[(\text{CH}_3)_4\text{N}]_2\text{M}_2\text{Ge}_4\text{S}_{10}$ showing the 3D zinc blende-type of open-framework structure, in which the tetrahedral Zn^{2+} and S^{2-} sites are alternately substituted by metal–metal bonded dimetal Ag_2^{2+} or Cu_2^{2+} and adamantanoid $\text{Ge}_4\text{S}_{10}^{4-}$ building-blocks, all covalently linked together by $[\text{Ge}(\mu\text{-S})_2\text{M}-\text{M}(\mu\text{-S})\text{Ge}]_2$ bridge bonds. The encapsulated $[(\text{CH}_3)_4\text{N}]^+$ cations have been removed from the illustrations for clarity. Graphics color code: Ge, purple; S, yellow; M (M = Ag, Cu), green.

Room-temperature X-ray powder diffraction data were collected on a Siemens D-5000 diffractometer using a Cu tube source and a “drifted Li-Si” solid-state detector whose energy window was centered at 8.04 keV. The detector was set to discriminate against β , leaving the $\alpha_{1,2}$ X-ray lines. Voltage and current settings of the X-ray tube were 50 kV and 35 mA, respectively. The samples were packed onto low background flat plates. For practical reasons the data were collected in two sections, from 10 to 42° and from 42 to $75^\circ 2\theta$. This allowed the collection of high signal-to-noise data in the upper range while still keeping total collection times within acceptable limits for the X-ray facility. The Rietveld refinements were carried out using the general structure analysis system (GSAS).⁴ The two ranges of each data set were fitted as two histograms for a single structural model. The unit-cell starting values were obtained from indexing the lower range histogram.

Table 1. Unit-Cell Parameters (Å)

metal	<i>a</i>	<i>c</i>
Cu	9.51(1)	15.02(2)
Ag	9.550(8)	15.09(1)

The single-crystal data⁵ for $[(\text{CH}_3)_4\text{N}]_2\text{MnGe}_4\text{S}_{10}$ were used to provide the initial atom positions within the unit cell and the $\bar{I}\bar{4}$ space group. The atom positions were translated within the unit cell to place a $\text{Ge}_4\text{S}_{10}^{4-}$ unit at the body center, rather than a $[(\text{CH}_3)_4\text{N}]^+$. This allowed easier monitoring of the structure integrity during refinement. The histograms were fit by first refining the lattice parameters and the background function. Next the atom positions were allowed to vary, and then peak profile coefficients. The peaks were modeled as pseudo-Voigt functions. The starting values for the coefficients were determined by refining LaB_6 ,⁶ a line-shape standard. Isotropic temperature factors were constrained to positive values. Any factor that ran negative was replaced with GSAS's default value of 0.0250 and fixed before final refinement. The $[(\text{CH}_3)_4\text{N}]^+$ cations present in the void spaces of the framework were fit as “ NC_4 rigid bodies” which maintain their structure. No attempt was made to fit the $[(\text{CH}_3)_4\text{N}]^+$ cations with the hydrogens attached since past experience with room-temperature data Rietveld refinements has demonstrated no improvement in the correlation of the results to those obtained by single-crystal diffraction methods. Efforts to fit the $[(\text{CH}_3)_4\text{N}]^+$ as independent atoms caused fragmentation of the molecule. This resulted from slight background electron density within the cavity. The most reasonable explanation is some delocalization of the $[(\text{CH}_3)_4\text{N}]^+$ cations about the special positions on which they are centered. All the refinements gave R_p values of less than 10% indicating acceptable fits. See tables for details.

Results and Discussion

PXRD patterns have been recorded for $[(\text{CH}_3)_4\text{N}]_2\text{M}_2\text{Ge}_4\text{S}_{10}$ ($\text{M} = \text{Cu, Ag}$) under high-resolution low-temperature conditions on the National Synchrotron Light Source at Brookhaven National Laboratories, as well as with a Siemens D5000 X-ray diffractometer. The room-temperature PXRD patterns in both cases refined in the tetragonal space group $\bar{I}\bar{4}$ and yielded unit cell dimensions of $a = 9.550(8)$ Å and $c = 15.09(1)$ Å for silver and $a = 9.51(1)$ Å and $c = 15.02(2)$ Å for copper. There were no statistical differences between the room-temperature Siemens and the low-temperature synchrotron refinements (Tables 1–5). The mildness of the synthesis combined with the similarity of the powder pattern to those for $[(\text{CH}_3)_4\text{N}]_2\text{MeGe}_4\text{S}_{10}$ ($\text{Me} = \text{Mn, Fe}$)^{3,7} suggested that the structures might be similar, that is, composed of $\text{Ge}_4\text{S}_{10}^{4-}$ clusters linked through divalent single metal sites. This turned out not to be the case.

With the $[(\text{CH}_3)_4\text{N}]_2\text{MnGe}_4\text{S}_{10}$ single-crystal XRD structure⁵ as a starting model, a Rietveld PXRD full-profile structure analysis was performed on $[(\text{CH}_3)_4\text{N}]_2\text{Ag}_2\text{Ge}_4\text{S}_{10}$. The structure based upon single Ag^+ connecting units would only refine down to an R_p factor of about 17%. A Fourier electron density difference map performed with the Ag^+ removed from the framework clearly revealed the presence of two Ag^+ centers having

(4) Larson, A. C.; Von Dreele, R. B. Los Alamos Laboratory Report No. LA-UR-86-748, 1987.

(5) Yaghi, O. M.; Sun, Z.; Richardson, D. A.; Groy, T. L. *J. Am. Chem. Soc.* **1994**, *116*, 807–808. Achak, O.; Bivan, J. Y.; Maunaye, M.; Louër, D.; Louër, M. *J. of Alloys and Compounds*, **1995**, *219*, 111–115.

(6) National Institute of Standards and Technology instrument line position and profile shape (SRM 660) LaB_6 diffraction standards.

(7) Bowes, C. B.; Lough, A. J.; Malek, A.; Ozin, G. A.; Petrov, S.; Young, D. *Chem. Ber.* **1996**, *129*, 283–287.

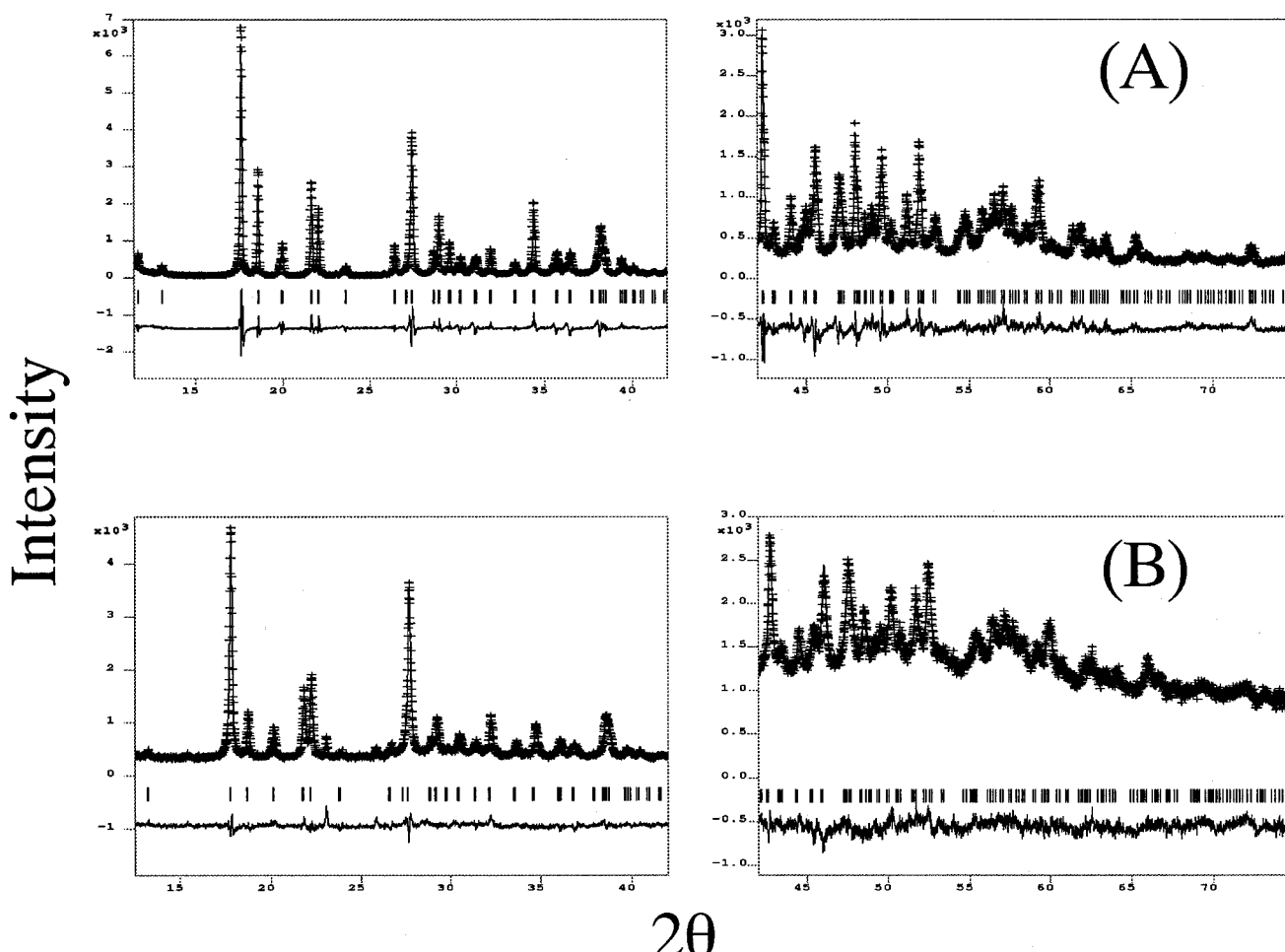


Figure 2. Observed (+, I_o), calculated (---, I_c) and difference ($I_o - I_c$) Siemens D5000 RT PXRD patterns of (A) $[(CH_3)_4N]_2Ag_2Ge_4S_{10}$ and (B) $[(CH_3)_4N]_2Cu_2Ge_4S_{10}$. Left and right plots represent histograms from $12.5-42^\circ$ and $42-75^\circ 2\theta$.

Table 2. Atom Parameters for $[(CH_3)_4N]_2Cu_2Ge_4S_{10}$

atom	<i>X</i>	<i>Y</i>	<i>Z</i>	isotropic temp factor
Ge	0.5805(5)	0.3295(4)	0.0857(3)	0.0250
S	0.6643(9)	0.1534(8)	0.1659(8)	0.0250
S	0.7509(8)	0.3977(7)	0.9918(8)	0.0250
S	0.5000	0.5000	0.179(1)	0.0250
N	0.0000	0.5000	0.2500	0.0250
C	0.079(5)	0.422(5)	0.194(2)	0.0250
N	0.0000	0.0000	0.0000	0.0250
C	0.051(3)	0.114(2)	0.064(2)	0.0250
Cu	0.5000	0.0000	0.1698(4)	0.0250

Table 3. Rietveld Refinement Statistics for $[(CH_3)_4N]_2Cu_2Ge_4S_{10}$

	R_{wp} (%)	R_p (%)
histogram 1	7.74	5.80
histogram 2	4.60	3.66
powder totals	5.59	4.21
χ^2_R	2.972	

electron density on the $\bar{4}$ axis, disposed symmetrically above and below the anticipated pseudotetrahedral Ag^+ lattice site. With these positions for the two neighboring Ag^+ centers, the 3D open-framework zinc blende lattice model proceeded to refine well to yield a final R_p factor of 9.92%, indicative of a reliable structure determination (Figure 2A). The data for $[(CH_3)_4N]_2Cu_2Ge_4S_{10}$ were refined using the results from the silver material as a starting point. The Rietveld analysis gave an R_p of 4.21%, (Figure 2B). Pertinent graphical projections of the determined crystal structures of $[(CH_3)_4N]_2Ag_2Ge_4S_{10}$ and $[(CH_3)_4N]_2Cu_2Ge_4S_{10}$ are shown in Figure 1B.

Table 4. Atom Parameters for $[(CH_3)_4N]_2Ag_2Ge_4S_{10}$

atom	<i>X</i>	<i>Y</i>	<i>Z</i>	isotropic temp factor
Ge	0.5836(5)	0.3333(5)	0.0822(3)	0.0250
S	0.6785(9)	0.1742(8)	0.1660(6)	0.0250
S	0.7513(8)	0.4185(8)	-0.0059(9)	0.0250
S	0.5000	0.5000	0.1833(9)	0.0250
N	0.0000	0.5000	0.2500	0.4(1)
C	0.079(5)	0.422(5)	0.194(2)	0.13(2)
N	0.0000	0.0000	0.0000	0.0250
C	0.051(3)	0.114(2)	0.064(2)	0.0250
Ag	0.5000	0.0000	0.1586(3)	0.067(2)

Table 5. Rietveld Refinement Statistics for $[(CH_3)_4N]_2Ag_2Ge_4S_{10}$

	R_{wp} (%)	R_p (%)
histogram 1	16.85	12.97
histogram 2	10.35	8.24
powder totals	13.03	9.92
χ^2_R	6.453	

The notably short distance between the two neighboring crystallographically equivalent M^+ centers in $[(CH_3)_4N]_2M_2Ge_4S_{10}$ refined to a value of 2.761 Å for silver and 2.409 Å for copper. These metal–metal distances are shorter than those of the bulk metals⁸ (2.89 Å, Ag; 2.54 Å, Cu) and lie at the low end of the ranges reported for silver and copper cluster compounds, that is, 2.73–3.00 and 2.40–2.79 Å, respectively.⁸ They are longer than the metal–metal bond lengths of the ns¹–ns¹ bonded gaseous dimers (2.486 Å Ag₂; 2.217 Å,

Cu_2 .⁹ Every M^+ center is coordinated to a terminal sulfide of two neighboring adamantanoid $\text{Ge}_4\text{S}_{10}^{4-}$ building blocks, at a distance of 2.373 Å for silver and 2.140 Å for copper, as well as to the adjacent M^+ center. These bond lengths imply covalent linking of the $\text{Ge}_4\text{S}_{10}^{4-}$ clusters by $[\text{Ge}(\mu\text{-S})_2\text{M}-\text{M}(\mu\text{-S})\text{Ge}]_2$ bridge bonds. The S–Ag–S and Ag–Ag–S angles are 174.6 and 87.3°, respectively, while the corresponding angles for copper are 176.8 and 91.6°. The $\text{S}_2\text{M}-\text{MS}_2$ linking moiety has dihedral symmetry with the terminal MS_2 units orthogonal to one another, like a “twisted I”. Charge-balance in these materials involves the anionic framework $[\text{M}_2\text{Ge}_4\text{S}_{10}]^{2-}$ and two $[(\text{CH}_3)_4\text{N}]^+$ template cations that reside within the cavities of the framework. The encapsulated $[(\text{CH}_3)_4\text{N}]^+$ cations were fit as rigid bodies with the N placed on two of the 4 special positions. There appears to be slight disorder of the $[(\text{CH}_3)_4\text{N}]^+$ about these positions in the room-temperature data. Their presence was confirmed by both the elemental and thermogravimetric analyses. This established the empirical formula of both materials to be $[(\text{CH}_3)_4\text{N}]_2\text{M}_2\text{Ge}_4\text{S}_{10}$ with essentially zero imbibed water.

Note that the Cu–Cu/Cu–S bonds in $[(\text{CH}_3)_4\text{N}]_2\text{Cu}_2\text{Ge}_4\text{S}_{10}$ are contracted by 0.352 Å/0.233 Å relative to the Ag–Ag/Ag–S ones in $[(\text{CH}_3)_4\text{N}]_2\text{Ag}_2\text{Ge}_4\text{S}_{10}$; however, the unit-cell dimensions are about the same. This apparent dichotomy can be understood by recognizing that the V-caps of the S–M–S “I” are normal ($>\text{-}<$) for $\text{M} = \text{Cu}$ and inverted ($<\text{-}>$) for $\text{M} = \text{Ag}$. Thus, the “I” flexibility compensates for the spatial demands of the $[(\text{CH}_3)_4\text{N}]^+$ and the lengths of the M–M/M–S bonds.

$[(\text{CH}_3)_4\text{N}]_2\text{Ag}_2\text{Ge}_4\text{S}_{10}$ and $[(\text{CH}_3)_4\text{N}]_2\text{Cu}_2\text{Ge}_4\text{S}_{10}$ represent the first examples of “dimetal” linked open-framework materials. They both contain metal–metal bonds with lengths shorter than the respective bulk metals. It is interesting that on increasing the spatial demands of the template, by changing $[(\text{CH}_3)_4\text{N}]^+$ in $[(\text{CH}_3)_4\text{N}]_2\text{Cu}_2\text{Ge}_4\text{S}_{10}$ to $[(\text{CH}_3\text{CH}_2)_4\text{N}]^+$, a material is obtained with the same stoichiometry, namely, $[(\text{CH}_3\text{CH}_2)_4\text{N}]_2\text{Cu}_2\text{Ge}_4\text{S}_{10}$, and a copper germanium sulfide 3D open-framework structure.¹⁰ However, the space group has changed from $\bar{I}4$ to $\bar{I}42d$ and the $\text{Ge}_4\text{S}_{10}^{4-}$ clusters in $[(\text{CH}_3\text{CH}_2)_4\text{N}]_2\text{Cu}_2\text{Ge}_4\text{S}_{10}$ have twisted and moved apart compared to those in $[(\text{CH}_3)_4\text{N}]_2\text{Cu}_2\text{Ge}_4\text{S}_{10}$. Concomitantly, the Cu–Cu internuclear separation has increased from its “bonding” distance of 2.409 Å in $[(\text{CH}_3)_4\text{N}]_2\text{Cu}_2\text{Ge}_4\text{S}_{10}$ to a “nonbonding” value of 6.947 Å in $[(\text{CH}_3\text{CH}_2)_4\text{N}]_2\text{Cu}_2\text{Ge}_4\text{S}_{10}$. Clearly the spatial demands of the template appears to control the distance between the metal linking sites in these open-framework materials.

It is well documented that $d^{10}\text{Ag}^+$ and Cu^+ cations in many oxide-, sulfide-, and halide-based materials can interact with each other in a way that influences both structure and physical properties.⁸ One finds cluster-like assemblies of $d^{10}\text{M}^+$ cations that correspond in geometry and bond lengths to “little pieces of metal”. The general consensus regarding the M^+-M^+ bonding in these $d^{10}-d^{10}$ aggregates is that the nd^{10} electrons have lost their core character and their interactions can be ascribed to the mixing of the closed-shell nd^{10} ground state with low-lying excited $(n+1)s$ and $(n+1)p$ states.⁸

(9) Stoll, H.; Fuentealba, P.; Dolg, M.; Flad, J.; Szentpaly, L. V.; Preuss, H. *J. Chem. Phys.* **1983**, *79*, 5532–5542.

(10) Tan, K.; Darovsky, A.; Parise, J. B. *J. Am. Chem. Soc.* **1995**, *117*, 7039–7040.

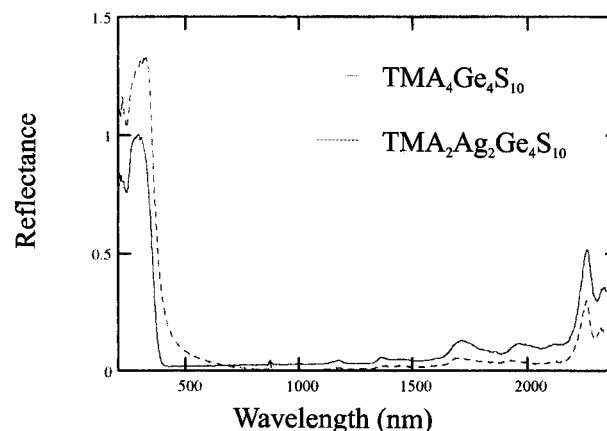


Figure 3. UV–vis–near-IR reflectance spectra of $[(\text{CH}_3)_4\text{N}]_2\text{Ag}_2\text{Ge}_4\text{S}_{10}$ (dash) and the precursor $[(\text{CH}_3)_4\text{N}]_4\text{Ge}_4\text{S}_{10}$ (solid).

Orgel was the first to suggest a valence-bond model to describe the bonding in compounds of $d^{10}\text{Ag}^+$ and Cu^+ cations.⁸ He postulated orthogonal hybrid orbitals $(1/\sqrt{2})(nd_z + (n+1)s)$ and $(1/\sqrt{2})(nd_z - (n+1)s)$. Jørgensen proposed that linear coordination of $d^{10}\text{M}^+$ cations is favored by a small energy separation between the ground-state $^1\text{S}_0$ and the first excited-state $^3\text{D}_3$.⁸ Hoffmann and Burdett showed that bonding interactions between fully occupied d shells of $nd^{10}\text{M}^+$ could arise if single-electron d functions were allowed to have partial $(n+1)s$ and $(n+1)p$ character.⁸ In the many recorded cases of materials containing Ag^+ and Cu^+ aggregates with $d^{10}-d^{10}$ interactions, some have intracluster metal–metal distances shorter than in the bulk metal.

The metal–metal bond lengths determined for the $d^{10}-d^{10}$ moiety $\text{S}_2\text{M}-\text{MS}_2$ in $[(\text{CH}_3)_4\text{N}]_2\text{M}_2\text{Ge}_4\text{S}_{10}$ are on the low end of their ranges.⁸ It is likely that destabilizing repulsive interactions between the three encapsulated cations ($2[(\text{CH}_3)_4\text{N}]^+/\text{M}^+$) in the hypothetical framework $[(\text{CH}_3)_4\text{N}]_2\text{M}\text{MGe}_4\text{S}_{10}$ drives the structure to the thermodynamically stable observed framework $[(\text{CH}_3)_4\text{N}]_2\text{M}_2\text{Ge}_4\text{S}_{10}$. Here intercation repulsions are reduced and $d^{10}-d^{10}\text{M}^+-\text{M}^+$ interactions are optimized. The geometry, bond lengths and bond angles of the $\text{S}_2\text{M}-\text{MS}_2$ “twisted I” in $[(\text{CH}_3)_4\text{N}]_2\text{M}_2\text{Ge}_4\text{S}_{10}$ are consistent with the involvement of $d^{10}-d^{10}$ orthogonal hybrid M^+-M^+ orbitals, $(1/\sqrt{2})(nd_z + (n+1)s)$ and $(1/\sqrt{2})(nd_z - (n+1)s)$, participating in the overall $\text{M}-\text{M}/\text{M}-\text{S}$ bonding scheme.

This structure–bonding picture facilitates the interpretation of some optical reflectance and FT Raman spectra recorded for $[(\text{CH}_3)_4\text{N}]_2\text{M}_2\text{Ge}_4\text{S}_{10}$. A representative UV–vis–near-IR spectral trace for $[(\text{CH}_3)_4\text{N}]_2\text{Ag}_2\text{Ge}_4\text{S}_{10}$ is shown in Figure 3. Included in Figure 3 is a spectrum of the precursor $[(\text{CH}_3)_4\text{N}]_4\text{Ge}_4\text{S}_{10}$. The latter displays a broad intense ultraviolet HOMO to LUMO transition around 315 nm with a rising edge beginning around 390 nm. A collection of weak near-IR absorptions are observed around 1150, 1350, 1700, 1850, 2100, 2250, 2300, and 2350 nm, associated with observed overtone and combination vibrational bands of the $[(\text{CH}_3)_4\text{N}]^+$ template cations (they correlate well with Raman spectra). The framework $[(\text{CH}_3)_4\text{N}]_2\text{Ag}_2\text{Ge}_4\text{S}_{10}$ shows a similarly intense broad ultraviolet absorption but red-shifted to around 360 nm with a rising edge commencing around 440 nm. Also the overtone and combination vibrational bands of the encapsulated $[(\text{CH}_3)_4\text{N}]^+$ template cations are present at essentially

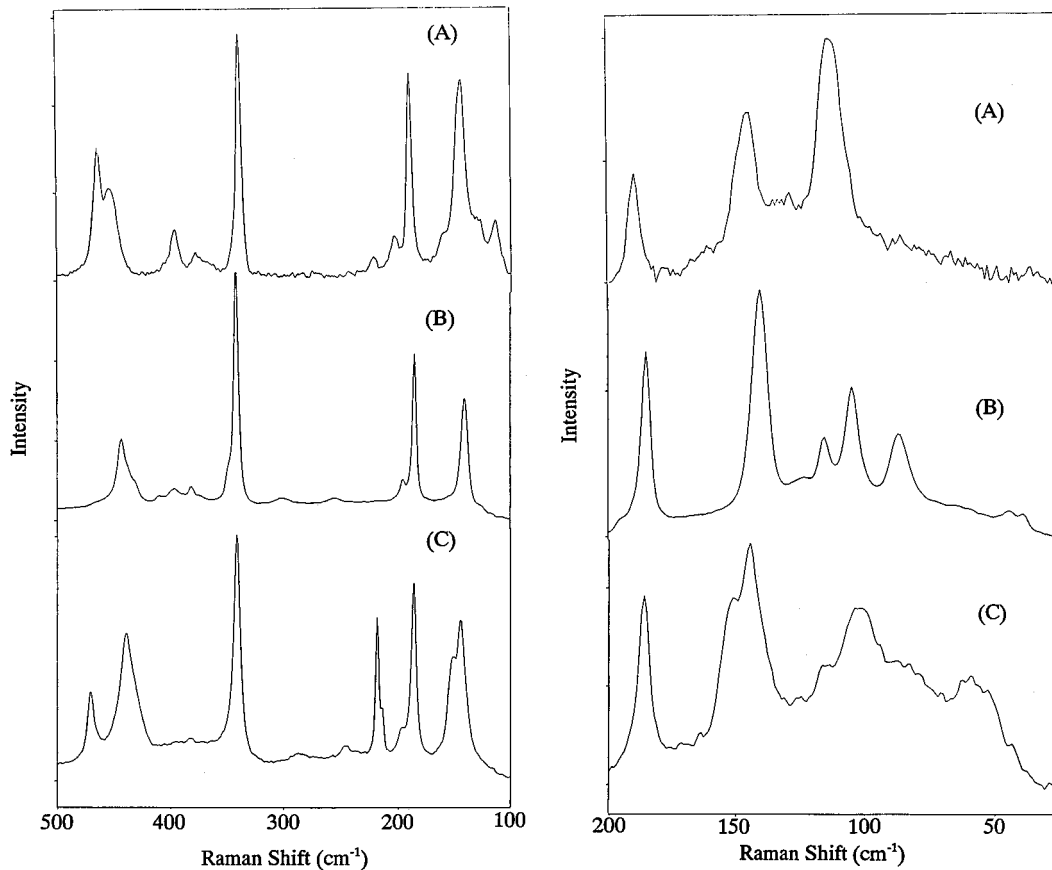


Figure 4. FT Raman spectra of (A) the precursor $[(\text{CH}_3)_4\text{N}]_4\text{Ge}_4\text{S}_{10}$, (B) $[(\text{CH}_3)_4\text{N}]_2\text{Ag}_2\text{Ge}_4\text{S}_{10}$, (C) $[(\text{CH}_3)_4\text{N}]_2\text{Cu}_2\text{Ge}_4\text{S}_{10}$. Left: 500–100 cm^{-1} . Right: 200–25 cm^{-1} .

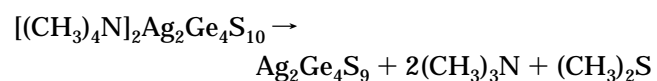
the same positions as those observed in the precursor $[(\text{CH}_3)_4\text{N}]_4\text{Ge}_4\text{S}_{10}$. On the basis of previous optical reflectance studies of materials containing aggregates of d^{10} Ag^+ cations,⁸ there are two main candidates for assigning the origin of the ultraviolet absorption. One involves electronic transitions between a valence band with predominantly Ag(I) 4d orbital character and a conduction band with mainly Ag(I) 5s and 5p orbital character. The other possibility involves transitions between a S(II) valence band and a conduction band with mainly Ag(I) 5s and 5p orbital character. Without further work and insight from high-level band structure calculations it is not easy to decide which of these two possibilities is correct.

For the precursor $[(\text{CH}_3)_4\text{N}]_4\text{Ge}_4\text{S}_{10}$, characteristic $[(\text{CH}_3)_4\text{N}]^+$ and $\text{Ge}_4\text{S}_{10}^{4-}$ vibrational modes occur in the FT Raman spectrum over the range of 4000–25 cm^{-1} . They remain essentially invariant on passing to the framework $[(\text{CH}_3)_4\text{N}]_2\text{M}_2\text{Ge}_4\text{S}_{10}$. Diagnostic modes occur for both precursor and framework in the ranges 464–339 and 223–114 cm^{-1} , respectively (Figure 4). Correlation coupling between $\text{Ge}_4\text{S}_{10}^{4-}$ modules in the $\text{I}\bar{4}$ tetragonal unit cell is weak, and they essentially behave like local cluster oscillators. In the window between the 464–339 and 223–114 cm^{-1} $\text{Ge}_4\text{S}_{10}^{4-}$ cluster modes, one observes the three expected ν_{MS} ($\text{A} + \text{B} + \text{E}$) Raman active $\text{S}_2\text{M} - \text{MS}_2$ “twisted I ” local modes (site symmetry S_4) at 298, 260, 252 cm^{-1} ($\text{M} = \text{Ag}$) and 283, 242, 214 cm^{-1} ($\text{M} = \text{Cu}$). Two bands at 41/35 cm^{-1} (Ag) and 57/52 cm^{-1} (Cu) are believed to be the ν_{MM} ($\text{A} + \text{B}$) Raman active ($Z = 2$, correlation couplet) metal–metal framework symmetrical breathing modes. On the basis of the 192/265 cm^{-1} vibrational frequencies reported for gaseous Ag/Cu_2 ,⁹ a local oscil-

lator calculation places the metal–metal framework breathing modes in this region.

To gain insight into the stability of this class of dimetal linked open-framework materials, with respect to the removal of the $[(\text{CH}_3)_4\text{N}]^+$ template, we have investigated the thermochemical properties of $[(\text{CH}_3)_4\text{N}]_2\text{Ag}_2\text{Ge}_4\text{S}_{10}$ by TGA, MS, and VT-PXRD. In a nitrogen atmosphere, the TGA shows sharp thermal transitions around 320 °C (20.5 wt %) and above 500 °C (4.1 wt %) followed by a broad thermal transition commencing around 600 °C and continuing beyond 700 °C (22 wt %, Figure 5). The water loss in this material occurs around 50 °C (0.5 wt %). This only corresponds to about 0.27 mol of H_2O per $[(\text{CH}_3)_4\text{N}]_2\text{Ag}_2\text{Ge}_4\text{S}_{10}$ and most likely arises from externally physisorbed water, consistent with the lack of observable change in the PXRD determined unit-cell dimensions of the template-containing material in air and under vacuum.

Mass spectroscopic examination of the volatiles evolved during the observed thermal events shows that mainly $(\text{CH}_3)_3\text{N}$ and $(\text{CH}_3)_2\text{S}$ accompany the 320 °C transition. The TGA shows this to correspond to roughly 2($\text{CH}_3)_3\text{N}$ and 1($\text{CH}_3)_2\text{S}$ per $[(\text{CH}_3)_4\text{N}]_2\text{Ag}_2\text{Ge}_4\text{S}_{10}$ formula unit. Therefore, the 320 °C event may be ascribed to the thermally driven “non-redox” template-loss reaction:



The 500 °C thermal event yields sublimed germanium sulfides. The products of this reaction are found to be PXRD amorphous.

The corresponding VT-PXRD studies of $[(\text{CH}_3)_4\text{N}]_2\text{Ag}_2\text{Ge}_4\text{S}_{10}$ under nitrogen shows that the material

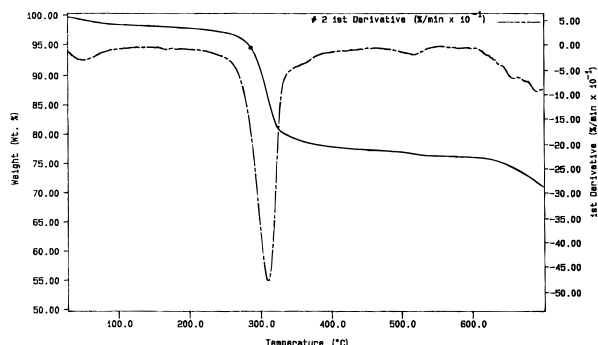


Figure 5. TGA-DTGA traces run under N_2 for $[(\text{CH}_3)_4\text{N}]_2\text{Ag}_2\text{Ge}_4\text{S}_{10}$.

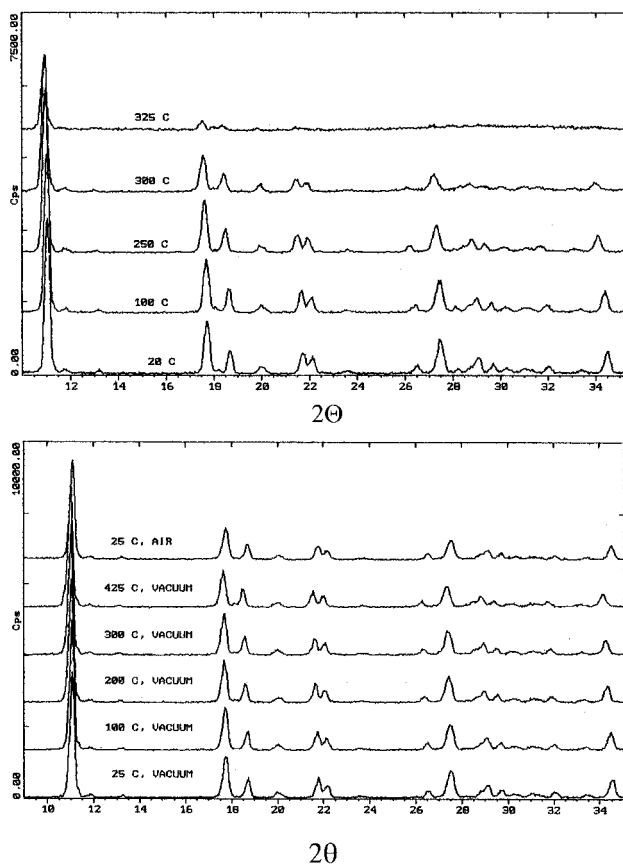


Figure 6. Variable-temperature in situ PXRD data for $[(\text{CH}_3)_4\text{N}]_2\text{Ag}_2\text{Ge}_4\text{S}_{10}$. Top: in N_2 . Bottom: in dynamic vacuum.

collapses at the 320°C thermal transition. By marked contrast, when the thermal treatment of $[(\text{CH}_3)_4\text{N}]_2\text{Ag}_2\text{Ge}_4\text{S}_{10}$ is conducted under vacuum it shows no sign of collapse up until about 480°C (Figure 6). Some line broadening begins to occur around 425°C . Under nitrogen, deleterious attack of the framework by reactive organic template fragments causes breakdown of the entire structure, whereas these effects are minimized under dynamic vacuum conditions. The vacuum thermally produced template-free $\text{Ag}_2\text{Ge}_4\text{S}_9$ material is at least as highly crystalline as the original template-containing $[(\text{CH}_3)_4\text{N}]_2\text{Ag}_2\text{Ge}_4\text{S}_{10}$ material. Moreover, it

is stable on cooling to room temperature in vacuum and in air. This is a significant difference from $[(\text{CH}_3)_4\text{N}]_2\text{MeGe}_4\text{S}_{10}$ ($\text{Me} = \text{Mn, Fe}$) where the framework is not stable after template removal.⁷ Much more work is required to establish the structural details and adsorption properties of the template-free material.

Conclusion

Synthetic and X-ray structural details, optical and vibrational spectroscopic, and thermal properties of the materials $[(\text{CH}_3)_4\text{N}]_2\text{M}_2\text{Ge}_4\text{S}_{10}$ (where $\text{M} = \text{Cu, Ag}$) are described for the first time. Rietveld PXRD full-profile structure refinements of $[(\text{CH}_3)_4\text{N}]_2\text{M}_2\text{Ge}_4\text{S}_{10}$ reveals a novel kind of zinc blende open-framework architecture in which the tetrahedral Zn^{2+} and S^{2-} sites are alternately substituted by dimetal M_2^{2+} and adamantanoid $\text{Ge}_4\text{S}_{10}^{4-}$ building blocks, all linked together by $[\text{Ge}(\mu-\text{S})]_2\text{M}-\text{M}[(\mu-\text{S})\text{Ge}]_2$ metal–metal bonded bridging units. The metal–metal distances in the $\text{S}_2\text{M}-\text{MS}_2$ “twisted I” dihedral unit are 2.761 \AA (Ag) and 2.409 \AA (Cu). Interestingly, these internuclear separations are shorter than the bulk metals themselves (2.89 \AA , Ag; 2.54 \AA , Cu). This implies that the adamantanoid $\text{Ge}_4\text{S}_{10}^{4-}$ -based open-framework structure is held together by $\text{d}^{10}-\text{d}^{10}\text{ M}^+-\text{M}^+$ metal–metal bonds. FT Raman provides a direct probe of this interaction. Metal–metal framework breathing vibrational modes are observed around 38 cm^{-1} for $\text{M} = \text{Ag}$ and 55 cm^{-1} for $\text{M} = \text{Cu}$. In situ VT-PXRD and TGA analyses demonstrate that $[(\text{CH}_3)_4\text{N}]_2\text{Ag}_2\text{Ge}_4\text{S}_{10}$ retains its structural integrity in vacuo until about 480°C . It seems likely that the disilver connection of adamantanoid $\text{Ge}_4\text{S}_{10}^{4-}$ building blocks confers thermal stability upon the framework. Ongoing investigations of dimetal linked open frameworks will focus attention on other metals (e.g., Au, Hg), their adsorption behavior, single-crystal and thin-film growth, electrical and photoconductivity properties, and the potential for molecule-discriminating chemical sensing.

Acknowledgment. The generous financial assistance of the Natural Sciences and Engineering Research Council of Canada (NSERC) and the Canadian Space Agency (CSA) is deeply appreciated. The scanning electron micrograph was collected by Dr. Neil Coombs (Imagetek) and the elemental analyses were performed by Dr. Walter Zamachek (UOP). Synchrotron PXRD data were collected at the National Synchrotron Light Source, Brookhaven National Laboratories which is supported by the United States Department of Energy, Division of Materials Sciences, and the Division of Chemical Sciences. FT-Raman spectra were recorded at the Ontario Laser and Lightwave Research Centre at the University of Toronto. C.L.B., S.J.K., and A.M. acknowledge NSERC for graduate scholarships and W.U.H. for undergraduate summer scholarships.

CM960280A